The coupling between ocean waves and rectangular ice sheets

R. Porter*

School of Mathematics, University Walk, University of Bristol, BS8 1TW, UK.

Abstract

This paper describes a semi-analytic approach to problems involving rectangular elastic plates of shallow draft floating on water. Specifically, two problems are considered: the scattering of plane monochromatic incident waves by a single elastic plate and the propagation/attenuation of waves through a periodic rectangular arrangement of plates. The approach combines Fourier methods with Rayleigh-Ritz methods for free modes of rectangular plates which reduces each problem to an algebraic system of equations which are are numerically accurate and efficient to compute. A selection of results are given to illustrate the work. The approach can be applied to many problems in hydroelasticity including the seakeeping of large flat-bottomed marine vessels, deflections in very large floating structures such as offshore airports and wave propagation through areas of broken sea ice.

Keywords: Floating ice, ocean wave scattering, periodic arrays, rectangular ice floes

1. Introduction

The propagation of energy through thin flexible ice sheets floating on water and its coupling to ocean wave energy is a research topic which has attracted significant recent attention; see, for example, the review article of Squire [20]. The principle application area relates the study of seasonal sea ice where interest centres on characterising the propagation of wave energy originating from the ocean through areas of broken ice and its effect on shore-fast sea ice [9]. Current models to predict attenuation rate of energy

*Corresponding author

Email address: richard.porter@bris.ac.uk (R. Porter)

(e.g. [11], [23], [24]) typically incorporate results from fundamental sea-ice/wave interaction problems. These include, for example, how energy is transmitted at water/ice sheet boundaries and across cracks, leads, pressure ridges and keels in ice sheets (e.g. [1], [22], [21], [5], [4], [25]). Lately, more sophisicated modelling has been performed on interaction effects between multiple three-dimensional ice floes and large regular or pseudo-random arrangements of ice floes (e.g. [16]). Scattering by more realistic ice floes which typically have jagged edges and are roughly polygonal are hard to compute, requiring discrete boundary/finite element-type calculations (e.g. [15], [17]). Consequently, researchers have typically resorted to using circular ice sheets for which semi-analytic methods (e.g. separation of variables and mode-matching) can be employed to speed up numerical calculations (e.g. [2], [3], [16]).

A second application area concerns the calculation of the wave response of large or very large floating structures such as large ships/barges, offshore airports and floating storage facilities. Fully-discretised numerical approaches coupling structural and hydrodynamic responses have been developed for these types of problems (see e.g. [8], [12], [7]) but a numerically very expensive. It is worth noting that, for the applications listed above, geometries are often approximately rectangular and of shallow draft.

This paper provides an account of a semi-analytical approach to solving a problem involving waves interaction with thin rectangular elastic plates floating on water. The work follows from two recent papers involving the current author. The first ([18]) considers ocean wave interaction with rigid rectangular plates of small draft and advocates the use of Fourier transforms methods as a simple, effective and numerically efficient procedure for computing solutions. The second ([14]) considers the the use of flexible floating plates with internal damping as a continuum model for articulated raft wave energy converters. One of the key contributions of the latter work was showing how the unknown deflection of the floating plate could be represented in terms of in-vacuo bending modes of a one-dimensional elastic plate. These can be determined explicitly and followed the cue from [13].

The foundation of the solution presented in this paper is based on those two previous pieces of work mentioned above and the detailed development of solutions presented in, for example, Section 2 of this paper are suppressed as a result. However, significant challenges remain. Unlike the solution used in [14] which assumed rectangular plates with flexibity in one direction (and rigid in a perpendicular direction), the elastic plate has isotropic properties. The unknown displacement of the plate is now expanded in the *in vacuo* eigenmodes for a thin rectangular plate with free edges whose solutions

cannot be expressed explicitly. Thus, our principle effort is in demonstrating how the numerical solution of the *in vacuo* problem, famously first solved by Ritz (see [6]) can be embedded into the solution of the problem with an underlying fluid.

In §2 we consider the problem of the scattering of incident waves by a rectangular ice sheet, using Fourier transforms to derive an integral equation for an unknown vertical displacement of the ice sheet, subject to constraints on its edges and corners. We then show how the approximation of that function using the eigenmodes for the corresponding thin plate can be used to determine a relatively simple and rapidly convergent system of algebraic equations.

In §3 we then consider wave propagation/attenuation in infinite doubly-periodic arrays of rectangular ice sheets. Here by the use of finite Fourier transforms (Fourier series) replace infinite transforms and result in a similar system of equations to those derived in §2. The work is summarised in §4.

2. Scattering of ocean waves by a single rectangular ice floe

A thin ice sheet of constant thickness d and density ρ_i floats, with a draft assumed much smaller than other physical lengthscales including wavelength, on the surface of an ocean of infinite depth. The ice sheet is taken to be rectangular in shape and occupies the horizontal region $\mathcal{D} = \{(x,y)| -a < x < a, \ -b < y < b\}$ of the plane $z = 0$. The fluid, of density ρ_w, extends into $z < 0$. It is incompressible and inviscid and its motion is irrotational allowing the fluid motion to be described by a velocity potential which is written $\Re\{\phi(x,y,z)\mathrm{e}^{-\mathrm{i}\omega t}\}$ after assuming single frequency time dependence. Then ϕ satisfies

$$\Delta\phi = 0 \tag{2.1}$$

in the fluid where $\Delta = \nabla^2 + \partial_{zz}$ is the three-dimensional Laplacian and $\nabla^2 = \partial_{xx}+\partial_{yy}$ is its projection onto the horizontal plane. On the free surface of the ocean, the combined linearised dynamic and kinematic conditions give

$$\phi_z - K\phi = 0, \qquad z = 0, \ (x,y) \notin \mathcal{D} \tag{2.2}$$

where $K = \omega^2/g$; on the ice sheet, they result in

$$(D\nabla^2\nabla^2 + 1 - K\delta)\phi_z - K\phi = 0, \qquad z = 0, \ (x,y) \in \mathcal{D}. \tag{2.3}$$

In the above $D = Ed^3/(12\rho_w g(1-\nu^2))$ represents the bending stiffness terms of Young's modulus (E) and Poisson's ratio (ν) and $\delta = (\rho_i/\rho_w)d$ represents

heave inertia. Additional terms which represent the less significant effects of dissipation, compression and rotational inertia are not included in (2.3), but can be found in [1], for example.

The relationship between the vertical displacement of the surface $\Re\{\eta(x,y)\mathrm{e}^{-\mathrm{i}\omega t}\}$ and the potential is expressed by

$$\eta(x,y) = \frac{\mathrm{i}}{\omega}\phi_z(x,y,0). \tag{2.4}$$

This function is discontinuous across $\partial\mathcal{D} = \{|x| = a,\ |y| < b\ \cup\ |y| = b,\ |x| < a\}$ the boundary of $\mathcal{D}$ comprised of the the four straight edges of the ice sheet separating it from the ocean. These edges are free of bending moments and shear stresses which is represented by the conditions

$$\left.\begin{aligned}(\mathcal{B}\eta)(x,y) \equiv \eta_{nn} + \nu\eta_{ss} = 0,\\ (\mathcal{S}\eta)(x,y) \equiv \eta_{nnn} + (2-\nu)\eta_{nss} = 0,\end{aligned}\right\} \tag{2.5}$$

where n and s are used, respectively, to denote derivatives normal and tangential to the edge (consistently oriented). Additionally, the four corners are free of twisting moments and this implies that

$$\eta_{ns} = 0. \tag{2.6}$$

Finally far away from the ice sheet, $\phi_z \to 0$ as $z \to -\infty$, whilst a radiation condition requires that

$$\phi - \phi_{inc} \sim \text{outgoing waves at infinity} \tag{2.7}$$

where $\phi_{inc} = (-\mathrm{i}g/\omega)\mathrm{e}^{\mathrm{i}K(x\cos\theta_0 + y\sin\theta_0)}\mathrm{e}^{Kz}$ is the potential representing incident waves of unit amplitude propagating in the direction θ_0 measured anticlockwise from the positive x-axis.

An application of double Fourier transforms in x and y to the problem, following the work of [18], [14] leads to

$$\eta(x,y) - \frac{1}{4\pi^2}\int_{-\infty}^{\infty}\int_{-\infty}^{\infty}\frac{\sqrt{\alpha^2+\beta^2}}{\sqrt{\alpha^2+\beta^2}-K}P(\alpha,\beta)\mathrm{e}^{\mathrm{i}\alpha x}\mathrm{e}^{\mathrm{i}\beta y}\,\mathrm{d}\alpha\mathrm{d}\beta = \mathrm{e}^{\mathrm{i}K(x\cos\theta_0 + y\sin\theta_0)} \tag{2.8}$$

where

$$P(\alpha,\beta) = \int_{-b}^{b}\int_{-a}^{a}(K\delta - D\nabla^2\nabla^2)\eta(x,y)\mathrm{e}^{-\mathrm{i}\alpha x}\mathrm{e}^{-\mathrm{i}\beta y}\,\mathrm{d}x\mathrm{d}y. \tag{2.9}$$

Equations (2.1)–(2.4) have been used in deriving (2.8) whilst defining contours of integration in the inverse transform appropriately ensures (2.7) is also satisfied. The integrand in (2.8) is singular along the circle $\alpha^2+\beta^2 = K^2$. Transforming integration variables from α, β to polar coordinates with $\alpha = K\rho\cos\chi$, $\beta = K\rho\sin\psi$ allows us to identify singularities as simple poles at $\rho = 1$ on the real ρ-axis and choosing the inverse contour to pass below this pole allows (2.7) to be satisfied.

An integral equation determining $\eta(x, y)$, $(x, y) \in \mathcal{D}$, is arrived at by restricting (2.8) to $(x, y) \in \mathcal{D}$ but requires $\eta(x, y)$ to additionally satisfy (2.5) and (2.6) on $\partial\mathcal{D}$. Once $\eta(x, y)$ is determined in $\mathcal{D}$, (2.8) can be used for $(x, y) \notin \mathcal{D}$ to reconstruct the displacement of surrounding free surface.

In order to solve the integral equation for $\eta(x, y)$, we first write the right-hand side term in (2.8) as

$$\mathrm{e}^{\mathrm{i}K(x\cos\theta_0+y\sin\theta_0)} = \sum_{\mu,\nu=0,1} R^{(\mu\nu)}(x, y) \tag{2.10}$$

where

$$\begin{aligned} R^{(00)}(x, y) &= \cos(Kx\cos\theta_0)\cos(Ky\sin\theta_0), \\ R^{(01)}(x, y) &= \mathrm{i}\cos(Kx\cos\theta_0)\sin(Ky\sin\theta_0), \\ R^{(10)}(x, y) &= \mathrm{i}\sin(Kx\cos\theta_0)\cos(Ky\sin\theta_0), \\ R^{(11)}(x, y) &= -\sin(Kx\cos\theta_0)\sin(Ky\sin\theta_0). \end{aligned} \tag{2.11}$$

The response is decomposed in the same manner as

$$\eta(x, y) = \sum_{\mu,\nu=0,1} \eta^{(\mu\nu)}(x, y). \tag{2.12}$$

such that $\eta^{(\mu\nu)}(x, y) = (-1)^\mu\eta^{(\mu\nu)}(-x, y) = (-1)^\nu\eta^{(\mu\nu)}(x, -y) = (-1)^{\mu+\nu}$ $\eta^{(\mu\nu)}(-x, -y)$. These definitions match the symmetries of the functions $R^{(\mu\nu)}(x, y)$ about x and y axes.

We follow [14] exploiting an idea originally due to [13] in expanding the unknown plate deflection in terms of the eigenmodes of the unloaded thin elastic plate. That is, we write

$$\eta^{(\mu\nu)}(x, y) = \sum_{i=0}^{\infty} \frac{a_i^{(\mu\nu)}}{(K\delta - D\lambda_i^{(\mu\nu)})} W_i^{(\mu\nu)}(x, y) \tag{2.13}$$

where $a_i^{(\mu\nu)}$ are undetermined coefficients and the denominator is included for algebraic convenience. In (2.13) $W \equiv W_i^{(\mu\nu)}(x, y)$ and $\lambda \equiv \lambda_i^{(\mu\nu)}$ refer to

the ith eigenfunction/ eigenvalue pair of the eigenproblem

$$(\nabla^2\nabla^2 - \lambda)W = 0, \qquad (x,y) \in \mathcal{D} \tag{2.14}$$

satisfying $(\mathcal{B}W)(x,y) = (\mathcal{S}W)(x,y) = 0$ on $(x,y) \in \partial D$ and $W_{xy} = 0$ on the four corners of ∂D with symmetry/antisymmetry about $x = 0$ and $y = 0$ represented by $\mu = 0/1$ and $\nu = 0/1$.

The problem of determining the free modes and their frequencies for the oscillations of a thin rectangular elastic plate with free edges, represented in the eigenproblem above, has a long history. Separately available supplementary material (see [19]) provides the background to this problem and details of its numerical solution. In it, the free plate eigenmodes are approximated by writing

$$W_i^{(\mu\nu)}(x,y) \approx \sum_{m=0}^{N}\sum_{n=0}^{N} \alpha^{(i)}_{2m+\mu,2n+\nu} w_{2m+\mu}(x/a) w_{2n+\nu}(y/b) \tag{2.15}$$

where the coefficients $\alpha^{(i)}_{2m+\mu,2n+\nu}$ are determined numerically by the Rayleigh-Ritz method and where the functions $w_n(t)$ for $|t| < 1$ represent eigenmodes for the corresponding one-dimensional Euler-Bernoulli beam equation with free edges and are given by

$$w_0(t) = \sqrt{1/2}, \qquad w_1(t) = t\sqrt{3/2}, \tag{2.16}$$

with

$$w_{2n}(t) = \frac{1}{\sqrt{2}}\left(\frac{\cosh k_{2n}t}{\cosh k_{2n}} + \frac{\cos k_{2n}t}{\cos k_{2n}}\right), \quad (\tanh k_{2n} = -\tan k_{2n}) \tag{2.17}$$

for $n \geq 1$ and

$$w_{2n+1}(t) = \frac{1}{\sqrt{2}}\left(\frac{\sinh k_{2n+1}t}{\sinh k_{2n+1}} + \frac{\sin k_{2n+1}t}{\sin k_{2n+1}}\right), \quad (\tanh k_{2n+1} = \tan k_{2n+1}) \tag{2.18}$$

again, $n \geq 1$. The brackets contain the relations satisfied by k_n, an increasing sequence of positive values beyond k_1.

In [19] is it also shown that $W_i^{(\mu\nu)}(x,y)$ are orthogonal, in the sense

$$\frac{1}{ab}\int_{-b}^{b}\int_{-a}^{a} W_i^{(\mu\nu)}(x,y) W_j^{(\kappa\lambda)}(x,y)\mathrm{d}x\mathrm{d}y = E_j^{(\mu\nu)}\delta_{\mu\kappa}\delta_{\nu\lambda}\delta_{ij} \tag{2.19}$$

where

$$E_i^{(\mu\nu)} \approx \sum_{m=0}^{N}\sum_{n=0}^{N}\{\alpha^{(i)}_{2m+\mu,2n+\nu}\}^2 \tag{2.20}$$

is determined numerically in terms of coefficients $\alpha_{m,n}^{(i)}$ referred to above.

The representation of $\eta(x,y)$ in terms of eigenmodes of the free-edge plate problem expressed in (2.15) has two important features in the context of the current problem. First, it means that η satisfies the required conditions on the edges and corners of the ice sheet and, secondly, it allows the fourth-order differential operator $\nabla^2\nabla^2$ acting on $\eta(x,y)$ in (2.8) to be substituted by terms involving $\lambda_i^{(\mu\nu)}$ multiplying $W_i^{(\mu\nu)}$.

Thus, substituting (2.15) into (2.8) with (2.9) and (2.10) before multiplying through by $W_j^{(\kappa\lambda)}(x,y)$ and integrating over $(x,y)\in\mathcal{D}$ results in a system of equations satisfied by $a_i^{(\mu\nu)}$ as

$$\frac{E_j^{(\mu\nu)}a_j^{(\mu\nu)}}{K\delta - D\lambda_j^{(\mu\nu)}} - \sum_{i=0}^{\infty} a_i^{(\mu\nu)}Q_{i,j}^{(\mu\nu)} = R_j^{(\mu\nu)}, \qquad j=0,1,\ldots \tag{2.21}$$

and $\mu,\nu = 0,1$ after use of the orthogonality relation (2.19). Here

$$Q_{i,j}^{(\mu\nu)} = \frac{ab}{4\pi^2}\int_{-\infty}^{\infty}\int_{-\infty}^{\infty}\frac{\sqrt{\alpha^2+\beta^2}}{\sqrt{\alpha^2+\beta^2}-K}\mathfrak{W}_i^{(\mu\nu)}(\alpha,\beta)\mathfrak{W}_j^{(\mu\nu)}(-\alpha,-\beta)\mathrm{d}\alpha\mathrm{d}\beta \tag{2.22}$$

where

$$\mathfrak{W}_i^{(\mu\nu)}(\alpha,\beta) = \frac{1}{ab}\int_{-b}^{b}\int_{-a}^{a} W_i^{(\mu\nu)}(x,y)\mathrm{e}^{-\mathrm{i}\alpha x}\mathrm{e}^{-\mathrm{i}\beta y}\,\mathrm{d}x\mathrm{d}y \tag{2.23}$$

and

$$R_j^{(\mu\nu)} = \frac{1}{ab}\int_{-b}^{b}\int_{-a}^{a} W_j^{(\mu\nu)}(x,y)R^{(\mu\nu)}(x,y)\,\mathrm{d}x\mathrm{d}y. \tag{2.24}$$

Finally, we need to calculate the expressions for $\mathfrak{W}_i^{(\mu\nu)}(\alpha,\beta)$. It follows from (2.15) and (2.23) that

$$\mathfrak{W}_i^{(\mu\nu)}(\alpha,\beta) \approx \sum_{m=0}^{N}\sum_{n=0}^{N}\alpha_{2m+\mu,2n+\nu}^{(i)}\mathfrak{w}_{2m+\mu}(\alpha a)\mathfrak{w}_{2n+\nu}(\beta b) \tag{2.25}$$

where

$$\mathfrak{w}_m(\sigma) = \int_{-1}^{1} w_m(t)\mathrm{e}^{-\mathrm{i}\sigma t}\,dt. \tag{2.26}$$

With the definitions given in (2.16) and (2.17) it can be shown that $\mathfrak{w}_0(\sigma) = \sqrt{2}\sin\sigma/\sigma$, $\mathfrak{w}_1(\sigma) = -\mathrm{i}\sqrt{6}(\sin\sigma - \sigma\cos\sigma)/\sigma^2$, and, for $m>1$,

$$\mathfrak{w}_{2m}(\sigma) = \frac{2\sqrt{2}\sigma^2}{(\sigma^4 - k_{2m}^2)}(k_{2m}\cos\sigma\tanh k_{2m} + \sigma\sin\sigma) \tag{2.27}$$

and

$$\mathfrak{w}_{2m+1}(\sigma) = \frac{-\mathrm{i}2\sqrt{2}\sigma^2}{(\sigma^4 - k_{2m+1}^2)}(k_{2m+1}\sin\sigma\coth k_{2m+1} - \sigma\cos\sigma). \tag{2.28}$$

The limits $\sigma \to k_m$ exist in all cases. For computational purposes we use the evenness/oddness of $\mathfrak{w}_{2m}$ and $\mathfrak{w}_{2m+1}$ to restrict the integrals to $\alpha > 0$, $\beta > 0$ and convert integrals to polar coordinates (see earlier) before evaluating the contribution from the pole by shrinking the inverse Fourier transform contour onto the real axis

$$\begin{aligned} Q_{i,j}^{(\mu\nu)} = \frac{K^2ab}{\pi^2}\int_0^{\pi/2}\int_0^{\infty}\frac{\rho^2}{\rho-1}\mathfrak{W}_i^{(\mu\nu)}(K\rho\cos\chi, K\rho\sin\chi) \\ \mathfrak{W}_j^{(\mu\nu)}(-K\rho\cos\chi, -K\rho\sin\chi)\,d\rho d\chi \\ + \mathrm{i}\frac{K^2ab}{\pi}\int_0^{\pi/2}\mathfrak{W}_i^{(\mu\nu)}(K\cos\chi, K\sin\chi)\mathfrak{W}_j^{(\mu\nu)}(-K\cos\chi, -K\sin\chi)\,d\chi. \end{aligned} \tag{2.29}$$

The first integral in ρ is of a Cauchy principal-value type. Note that $Q_{i,j}^{(\mu\nu)} = Q_{j,i}^{(\mu\nu)}$. Also using the definitions above

$$R_j^{(\mu\nu)} = \mathfrak{W}_j^{(\mu\nu)}(-K\cos\theta_0, -K\sin\theta_0). \tag{2.30}$$

The displacement far from the ice sheet is described by the radiation condition

$$\eta(x,y) = \eta_{inc}(x,y) + \left(\frac{2}{\pi Kr}\right)^{1/2}\mathcal{A}(\theta;\theta_0)\mathrm{e}^{\mathrm{i}Kr-\mathrm{i}\pi/4} \tag{2.31}$$

in terms of the diffraction coefficient $\mathcal{A}(\theta;\theta_0)$ and $x = r\cos\theta$, $y = r\sin\theta$. From (2.7), considered in the limit $r \to \infty$ and matched to (2.31) through the use of stationary phase, it can be shown that

$$\mathcal{A}(\theta;\theta_0) = \frac{\mathrm{i}}{2}K^2ab\sum_{i=0}^{\infty}\sum_{\mu,\nu=0,1}a_i^{(\mu\nu)}R_i^{(\mu\nu)}. \tag{2.32}$$

Application of the optical theorem provides a relation

$$\int_0^{2\pi}|\mathcal{A}(\theta;\theta_0)|^2\,\mathrm{d}\theta = -\Re\{\mathcal{A}(\theta_0;\theta_0)\} \tag{2.33}$$

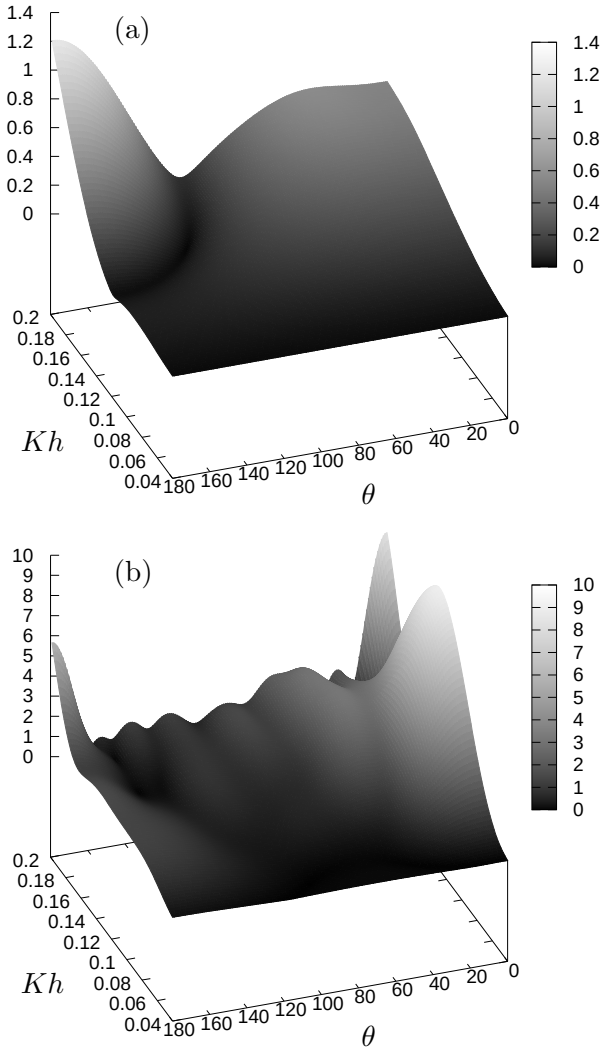

Figure 1: Diffraction coefficient amplitude $|\mathcal{A}(\theta;0)|$ measured against heading, θ, and frequency, Kh, for head incident waves. A square ice sheet is 1m thickness and dimension 20m in (a) and 80m in (b).

which can be used to check the accuracy of the numerical method. Numerically, this is found to be satisfied to 14 decimal places regardless of truncation of sums and integrals.

Numerically, we truncate sums over i, j to $J+1$ terms and typically

set $J = 4$. Then N is normally taken to be 4 or 5 and so the numerical method, while quite complicated to code, is actually very quick to run. For high accuracy, shorter wavelengths or larger elastic plates we chose larger values for the truncation parameters, always looking to achieve four decimal place accuracy. The highest values needed during testing of the results to maintain the accuracy required was $J = 8$ and $N = 12$.

In Fig. 1 we present the variation of the modulus of the diffraction coefficient $|\mathcal{A}(\theta; 0)|$ for head-incident waves with Kh and θ for square ice sheets. In both sub-figures, the ice sheet is $h = 1$m thick and we take $E = 6 \times 10^9$, $\rho_w = 1025\text{kgm}^3$, $\delta = (\rho_i/\rho_w)h = 0.9$ and $\nu = 0.3$, giving $D = 54645$. In the left-hand figure, $a = 10$m and in the right-hand figure, $a = 40$m. The range of values of Kh from 0.04 to 0.2 correspond to ocean wavelengths ranging from 157m to 31m or wave periods from 10s to 4.5s. Fig. 1 shows limited diffraction for wavelengths much longer than the ice floe.

Separate unpublished studies performed on two-dimensional scattering by finite length ice sheets suggest that 1m-thick ice sheet behaves approximately as a rigid floating plate for lengths under approximately 20m and that bending can have significant effects (depending on frequency) on scattering properties for 1m-thick ice sheets over 40m in length.

These observations are supported by the computations of the free surface illustrated in Fig. 2 for 20×20m and 80×80m ice sheets. In both cases, $Kh = 0.1$ is chosen, equivalent to 62m incident waves. Negligible bending is shown in the smaller ice floe (and this remains the case for other wavelengths), but it is noticeable in the larger ice sheet. Significant diffraction effects are also evident in Fig. 2(b) which tie in with the cross section through $Kh = 0.1$ in Fig. 1(b) of $|\mathcal{A}(\theta, 0)|$.

In Fig. 3 we consider wave scattering by elongated ice sheets. In both sub-figures, we consider an ice sheet of 1m thickness, of length 160m and width 40m whilst the incident wave is set at $Kh = 0.08$, equivalent to 73m incident wave length. The incident wave heading in Figs. 3(a) and (b) is 0° and 45°. It illustrates many expected features of diffraction; circular wave scattering, shadow and reflective zones. One can also observe the structure of bending waves (having a distinctive wavelength) within the ice sheet.

3. Wave propagation through a doubly-periodic array of rectangular ice sheets

Consider an infinite doubly-periodic array of identical thin floating ice sheets arranged on a rectangular lattice with periodicity $2A$ in the x direction and $2B$ in the y-direction. Each cell contains, within its borders, a single

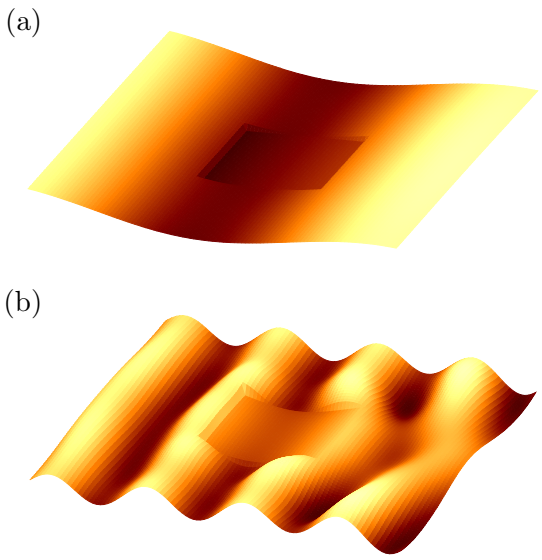

Figure 2: Surface elevation $\eta(x, y)$ for head incident waves on a 1m thickness ice sheet with $Kh = 0.1$ (wavelength 62m). In (a) and (b) the floe sizes are 20×20m and 80×80m.

rectangular ice floe of length $2a$ and width $2b$ and rotation ψ. When $\psi = 0$ the edges of the ice sheets are aligned with the underlying lattice. In such a case, choosing $a = A$ and $b = B$ results in a continuous covering of ice with cracks between adjacent ice sheets. With $a < A$ and $b < B$ leads are formed between them.

Using Bloch-Floquet theory we seek solutions which are quasi-periodic in both x and y, satisfying

$$\phi(x + 2A, y, z) = \mathrm{e}^{2\mathrm{i}\alpha_0 A}\phi(x, y, z), \qquad \phi_x(x + 2A, y, z) = \mathrm{e}^{2\mathrm{i}\alpha_0 A}\phi_x(x, y, z), \tag{3.1}$$

and

$$\phi(x, y + 2B, z) = \mathrm{e}^{2\mathrm{i}\beta_0 B}\phi(x, y, z), \qquad \phi_y(x, y + 2B, z) = \mathrm{e}^{2\mathrm{i}\beta_0 B}\phi_y(x, y, z), \tag{3.2}$$

for all $z < 0$ with identical spatial relations holding for the plate displacement $\eta(x, y) = (\mathrm{i}/\omega)\phi_z(x, y, 0)$. We refer to α_0 and β_0 as Bloch wavenumbers and these need only be considered between $0 < \alpha_0 A < \pi$, $0 < \beta_0 B < \pi$ as solutions with all other real values can be related solution within this range of values. It is typical to call $(\alpha_0 A, \beta_0 B)$ the dimensionless Bloch wavevector.

The problem to solve is now formed from (2.1)–(2.4) applied to a single ice sheet in a fundamental lattice cell, say $|x| < A$, $|y| < B$, with (3.1)

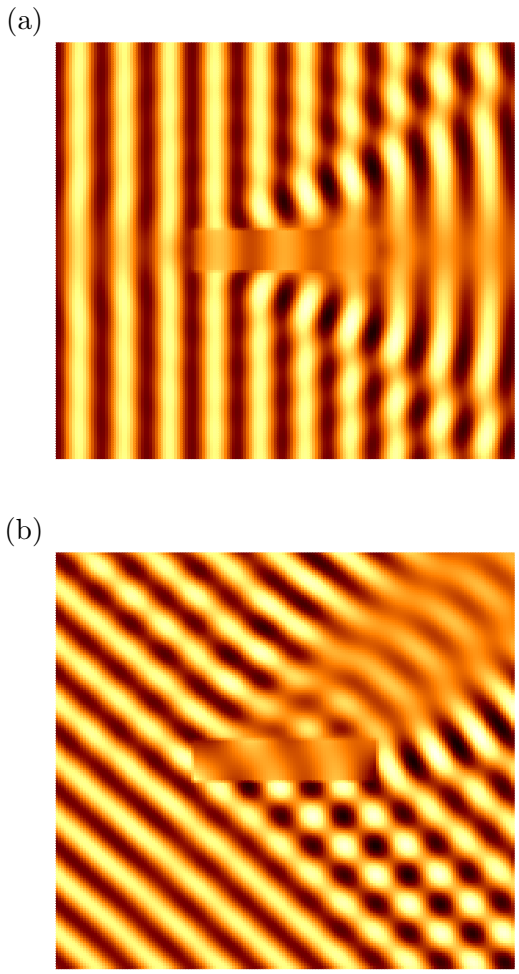

Figure 3: Surface elevation $\eta(x, y)$ for a wave heading of (a) 0° and (b) 45° on a 1m thickness ice sheet of length 160m and 40m width with $Kh = 0.08$ (wavelength 73m).

applying with $x = -A$ and (3.2) with $y = -B$ so as to constitute periodic boundary conditions connecting the solutions at the edges of the cell. Within the framework of this homogeneous problem, we seek non-trivial solutions which represent the propagation of free waves through the array. Specifically, we will seek values of frequency parameter K for which this occurs for a given Bloch wavevector, $(\alpha_0 A, \beta_0 B)$.

To solve the problem defined above we follow adopt the method of §2, re-

placing infinite Fourier transforms with finite Fourier transforms (or Fourier series). The most general expression satisfying (3.1) and (3.2) is given by

$$\phi(x,y,z) = \sum_{k=-\infty}^{\infty} \sum_{l=-\infty}^{\infty} A_{k,l}(z) \mathrm{e}^{\mathrm{i}\alpha_k x} \mathrm{e}^{\mathrm{i}\beta_l y} \tag{3.3}$$

where $A_{k,l}(z)$ is the (discrete in x, y) transform function and

$$\alpha_k = \alpha_0 + \frac{k\pi}{A}, \qquad \beta_l = \beta_0 + \frac{l\pi}{B}, \tag{3.4}$$

for all k, l. In accordance with the definition in (3.3) the finite Fourier transform of ϕ is defined as

$$A_{k,l}(z) = \frac{1}{4AB} \int_{-B}^{B} \int_{-A}^{A} \phi(x,y,z) \mathrm{e}^{-\mathrm{i}\alpha_k x} \mathrm{e}^{-\mathrm{i}\beta_l y} \,\mathrm{d}x\mathrm{d}y. \tag{3.5}$$

Satisfaction of Laplace's equation (2.1) along with $\phi_z \to 0$ as $z \to -\infty$ implies

$$A_{k,l}(z) = C_{k,l} \mathrm{e}^{\gamma_{k,l} z}, \qquad \gamma_{k,l} = \sqrt{\alpha_k^2 + \beta_l^2} \tag{3.6}$$

for arbitrary coefficients $C_{k,l}$ which are determined by taking the transform (3.5) of $\phi_z - K\phi$ on $z = 0$ and using conditions (2.2) and (2.3). This leads to

$$A_{k,l}(z) = \frac{P_{k,l} \mathrm{e}^{\gamma_{k,l} z}}{\gamma_{k,l} - K} \tag{3.7}$$

where

$$P_{k,l} = \frac{1}{4AB} \int_{-b}^{b} \int_{-a}^{a} (K\delta - D\nabla^2\nabla^2) \phi_z(x,y,0) \mathrm{e}^{-\mathrm{i}\alpha_k x} \mathrm{e}^{-\mathrm{i}\beta_l y} \,\mathrm{d}x\mathrm{d}y. \tag{3.8}$$

For clarity, we have assumed that the relative rotation of the ice sheet ϕ to that of the lattice is zero.

Now (3.7) represents the solution in transform space, expressed in terms of ϕ_z on $z = 0$. Taking the inverse, (3.3), a derivative in z and setting $z = 0$ gives the equation

$$\eta(x,y) = \frac{1}{4AB} \sum_{k=-\infty}^{\infty} \sum_{l=-\infty}^{\infty} \frac{\gamma_{k,l} \mathrm{e}^{\mathrm{i}\alpha_k x} \mathrm{e}^{\mathrm{i}\beta_l y}}{\gamma_{k,l} - K} \int_{-b}^{b} \int_{-a}^{a} (K\delta - D\nabla^2\nabla^2) \eta(x,y) \mathrm{e}^{-\mathrm{i}\alpha_k x} \mathrm{e}^{-\mathrm{i}\beta_l y} \,\mathrm{d}x\mathrm{d}y. \tag{3.9}$$

Values of (K, α_0, β_0) that satisfy this equation belong to dispersion surfaces which govern the relationship between frequency of motion and spatial periodicity in x and y of waves able to propagate indefinitely through the periodic array of ice sheets. In particular, those values of K for which no pairs $(\alpha_0 A, \beta_0 B)$ exist which satisfy (3.9) are said to belong to stop bands. If K does not belong to a stop band it is said to belong to a pass band and this implies that wave propagation allowed in at least some directions through the array. Solutions of (3.9) are sought in exactly the same way as for the single ice sheet, by expanding in series of eigenmodes. We write

$$\eta(x,y) = \sum_{\mu,\nu=0,1} \sum_{i=0}^{\infty} a_i^{(\mu\nu)} W_i^{(\mu\nu)}(x,y) \tag{3.10}$$

and this leads to the system of equations

$$\frac{E_j^{(\kappa\lambda)} a_j^{(\kappa\lambda)}}{K\delta - D\lambda_j^{(\kappa\lambda)}} - \sum_{\mu,\nu=0,1} \sum_{i=0}^{\infty} a_i^{(\mu\nu)} \widetilde{Q}_{i,j}^{(\mu\nu,\kappa\lambda)} = 0 \tag{3.11}$$

for $\kappa, \lambda = 0, 1$ where

$$\widetilde{Q}_{i,j}^{(\mu\nu,\kappa\lambda)} = \frac{ab}{4AB} \sum_{k=-\infty}^{\infty} \sum_{l=-\infty}^{\infty} \frac{\gamma_{k,l}}{\gamma_{k,l} - K} \mathfrak{W}_i^{(\mu\nu)}(\alpha_k, \beta_l) \mathfrak{W}_j^{(\kappa\lambda)}(-\alpha_k, -\beta_l) \tag{3.12}$$

and all other symbols are defined within §2.

There is not the same level of simplification as in §2 where the incident wave forcing was decomposed into the sum of four terms with different symmetries. In other words, there is now coupling between different symmetry modes in (3.12), essentially because of the offset in the Fourier modes introduced by quasi-periodicity sought in solutions.

In Fig. 4 we have plotted solutions of (3.11) in the case of $D = 54645$, $\delta = 0.9$, $a = 10$m, $a/A = b/B = 1$ and $a/b = 1.5$. The solutions form dispersion surfaces corresponding to propagating waves with the doubly-periodic array in frequency-Bloch wavevector space represented here by $(\alpha_0 A, \beta_0 B)$ on horizontal axes and KA along the vertical axis. In the literature, it is common to compress the information contained on these surface into the union of three cross-sections through the surfaces (the boundaries of the irreducible Broullion zone) to form a so-called band-gap diagram. Its main purpose is to to identify frequencies for which no waves may propagate, based on an assumption that minima and maxima in each dispersion surface are captured by this process. Such frequencies are then said to lie in a

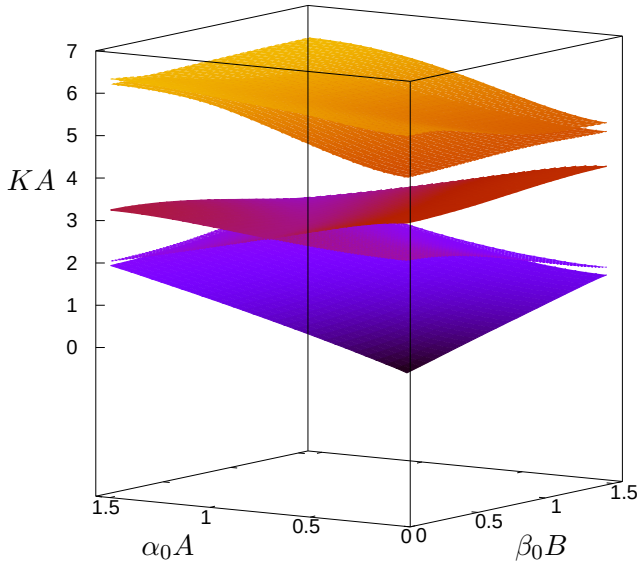

Figure 4: The first five dispersion surfaces (defined as relationship between the Bloch wavevector, $(\alpha_0 A, \beta_0 B)$, and frequency KA supporting wave propagation) for a doubly-periodic array of ice sheets: $D = 54645$, $a = 10$m, $a/A = b/B = 1$ and $a/b = 1.5$.

stop band. In the solution above there is a stop band between $kA = 3.95$ and $kA = 3\pi/2 \approx 4.71$. At other frequencies, within so-called pass bands, there are continuous ranges of values of Bloch wavevectors for which solutions exist and these relate to a range of possible phase relations as wave pass through the array. The slope of the dispersion surfaces, measured in the direction of the Bloch wavevector from the origin in Fig. 4 indicates the magnitude and direction group velocity of those waves. That is to say that the direction of energy transport is not always in the same direction as the Bloch wavevector. For point disturbances in the array, propagation of energy is only permitted in directions in which the Bloch wavevector and the group velocity vector are aligned. These are most often along the two perpendicular axes defining the lattice. For square lattices, radiation would also be expected along directions at 45 degrees to these lines; for non-square lattices radiation from point sources along other directions is less likely.

In Fig. 5 a perspective snapshot is shown of a section of the surface of an ice-covered ocean. In this example, $a/A = b/B = 1$ and $\psi = 0^\circ$ so that neighbouring ice sheets are separated by cracks. The parameters for this particular realisation are an ice thickness of $h = 1$m, $a = 20$m and

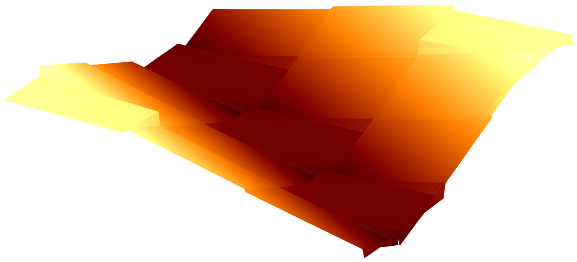

Figure 5: A section of the surface elevation $\eta(x,y)$ corresponding wave propagation through a doubly-periodic array of ice sheets. With $h = 1\text{m}$, $a = 20\text{m}$, $a/b = 1.5$, $a/A = b/B = 1$, $\psi = 0°$, $\alpha_0 A = \frac{1}{2}$, $\beta_0 B = \frac{1}{2}$ and $Kh = 0.04362$ is a solution on the first dispersion surface.

$a/b = 1.5$ so that individual ice sheets have dimensions $40 \times 26.3\text{m}$. The particular shown corresponds to Bloch wavenumbers of $\alpha_0 A = \beta_0 B = 0.5$ and $Kh = 0.04362$ is the solution which lies on the first dispersion surface and corresponds to low frequency (approximately 10 second) wave motions. It can be seen in Fig. 5 the ice sheets respond as rigid plates in this example as a consequence of their size and the long underlying wavelength which allows the individual floes to 'ride' the surface.

When the ice sheet is rotated by a non-zero angle ψ with respect to the underlying lattice, the changes that are needed result in a revised version of (3.11) being

$$\widetilde{Q}_{i,j}^{(\mu\nu,\kappa\lambda)} = \frac{ab}{4AB} \sum_{k=-\infty}^{\infty} \sum_{l=-\infty}^{\infty} \frac{\gamma_{k,l}}{\gamma_{k,l} - K} \mathfrak{W}_i^{(\mu\nu)}(\alpha'_k, \beta'_l) \mathfrak{W}_j^{(\kappa\lambda)}(-\alpha'_k, -\beta'_l) \quad (3.13)$$

where

$$\alpha'_k = \alpha_k \cos\psi + \beta_l (b/a) \sin\psi, \qquad \beta'_l = \beta_l \cos\psi - \alpha_k (a/b) \sin\psi \quad (3.14)$$

This results quite easily from a rotation of (x,y) coordinates through an angle ψ in (3.9)

In Fig. 6 we combine a rotation of the ice sheets with an opening up of the water surface between adjacent ice sheets resulting in open water channels or 'leads' between neighbouring ice sheets. We choose $h = 1\text{m}$ and $a/b = 1.5$ as before but with $a = 30\text{m}$ so that each ice sheet is $60 \times 40\text{m}$ in size. Here $a/A = b/B = 0.75$ and $\psi = 15°$ which allows each ice sheet to reside inside its own cell. The particular solution shown in Fig. 6 is for

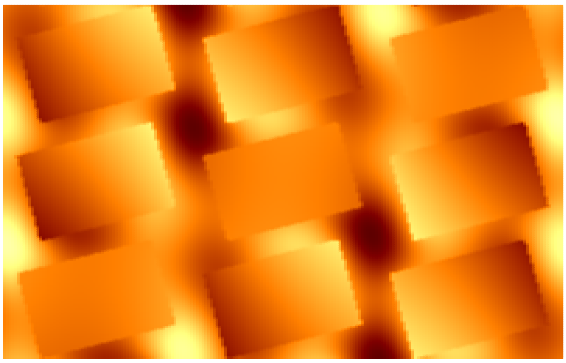

Figure 6: A section of the surface elevation $\eta(x, y)$ corresponding to wave propagation through a doubly-periodic array of ice sheets separated by open water leads. With $h = 1$m, $a = 30$m, $b = 20$m, $a/A = b/B = 0.75$, $\psi = 15^\circ$, $\alpha_0 A = 1$, $\beta_0 B = \frac{1}{2}$ and $Kh = 0.11889$ is a solution on the third dispersion surface.

$\alpha_0 A = 1$, $\beta_0 B = 0.5$ and a solution is taken from the third dispersion surface with $Kh = 0.11889$ equivalent to 6.78s-period motion. The motion is most easy visualised in plan view and there is a complicated interaction between water and ice sheets which can be seen to produce significant flexing of the ice sheets in the array.

Many similar types of results can easily be obtained and we have only shown two examples which highlight the main features which can be accessed.

4. Conclusions

In the first part of this paper we have described a semi-analytical approach to determine the response of a shallow-drafted rectangular elastic plate to waves. The application of Fourier transform methods results in an integral equation for the unknown displacement. This function is approximated in a numerical scheme using eigenmodes of the one-dimensional Euler-Bernoulli beam equation with numerically-determined weighting coefficients. This leads to a system of equations which is complicated to code, but one which is executed very quickly.

The coupling of numerically-determined in vacuo eigenmodes to the hydrodynamic problem is similar to other approaches; most notably that of [15]. There, a finite-element method discretisation of the elastic plate forms

the basis of the method; in this paper we use a spectral method which is computationally inexpensive for parameters of interest.

In the second part, the method is extended to doubly-periodic arrangements of ice sheets. Fourier series replace transforms and the result is a homogeneous infinite system of equations to determine wave modes propagating without attenuation through the array.

In both parts, a small selection of results serve to demonstrate the methods at work although there is no focus on any particularly new or unexpected wave phenomena. The existence of stop bands in periodic arrays of rectangular ice sheets may be of interest to some researchers interested in metamaterials. Extensions to the current work could include calculating interactions between finite arrays or singly-periodic arrays of rectangular ice floes.

[1] Balmforth, N.J. & Craster, R.V. (1999) Ocean waves and ice sheets *J. Fluid Mech.* **395**, 89–124.

[2] Bennetts, L.G., Peter, M.A., Squire, V.A. & Meylan, M.H. (2010) A three-dimensional model of wave attenuation in the marginal ice zone. *J. Geophys. Res.* **115**(C12)

[3] Bennetts L.G. & Williams T.D. (2015) Water wave transmission by an array of floating discs. *Proc. R. Soc. Lond. A* **471**:20140698.

[4] Chung, H. & Linton, C.M. (2005) Reflection and transmission across a finite gap in an infinite elastic plate on water. *Q.J. Mech. Appl. Math.* **58**, 1–15.

[5] Evans, D.V. & Porter, R. (2003) Wave scattering by narrow cracks in ice sheets floating on water of finite depth. *J. Fluid Mech.* **484**, 143–165.

[6] Gander, M. J. & Wanner, G., (2012), From Euler, Ritz, and Galerkin to modern computing. SIAM Review **54**(4) 627-666.

[7] Kashiwagi, M. (1998) A B-spline Galerkin scheme for calculating the hydroelastic response of a very large floating structure waves. *J. Mar. Sci. Tech.*, **3**(1) 37–49.

[8] Kim, K-H., Bang, J-S., Kim, J-H, Kim, Y., Kim, S-J & Kim, Y. (2013) Fully coupled BEM-FEM analysis for ship hydroelasticity in waves *Marine Structures* **33** 71–99.

[9] Kohout, A.L., Williams, M.J.M., Dean, S.M. & Meylan, M.H. (2014) Storm-induced sea-ice breakup and the implications for ice extent. *Nature* **509**(7502) 604–607.

[10] Kohout, A.L. & Meylan, M.H. (2006) A model for wave scattering in the marginal ice zone based on a two-dimensional floating-elastic-plate solution. *Ann. Glaciol.* **44**(1) 101–107.

[11] Kohout, A.L. & Meylan, M.H. (2008) An elastic plate model for wave attenuation and ice floe breaking in the marginal ice zone. *J. Geophys. Res.* **113** (C9)

[12] Lakshmynarayanana, P.A., Temarel, P. & Chen, Z. (2015) Hydroelastic analysis of a flexible barge in regular waves using coupled CFD-FEM modelling. *5th International Conference on Marine Structures (MARSTRUCT 2015), United Kingdom*. 95–103.

[13] Newman, J.N. (1994) Wave effects on deformable bodies. *Appl. Ocean Res.* **16**(1) 47–59.

[14] Noad, I.F. & Porter, R. (2017) Approximations to wave energy absorption by articulated rafts. *SIAM J. Appl. Maths* **77**(6) 2199-2223.

[15] Meylan, M.H. (2002) Wave response of an ice floe of arbitrary geometry. *J. Geophys. Res.* **107** (C1).

[16] Montiel, F. Squire, V.A. & Bennetts, L.G. (2015) Reflection and transmission of ocean wave spectra by a band of randomly distributed ice floes. *Ann. Glaciol.* **56**(69) 315–322.

[17] Peter, M.A. & Meylan, M.H. (2004) Infinite-depth interaction theory for arbitrary floating bodies applied to wave forcing of ice floes. *J. Fluid Mech.* **500** 145–167.

[18] Porter, R. (2016) Surface wave interaction with rigid plates lying on water. *Wave Motion* **66** 118–131.

[19] Porter, R. (2017) Eigenfrequencies and eigenmodes for a thin rectangular elastic plate with free edges. `http://people.maths.bris.ac.uk/~marp/abstracts/free-edge.pdf`

[20] Squire, V.A. (2007) Of ocean waves and sea-ice revisited. *Cold Reg. Sci. Tech.* **49**(2) 110–133.

[21] Squire, V.A. & Dixon, A.W. (2001) How a region of cracked sea ice affects ice-coupled wave propagation. *Ann. Glaciol.* **33** , 327–332.

[22] Tkacheva, L.A. (2001) Scattering of surface waves by the edge of a floating elastic plate. *J. Appl. Mech. Tech. Phys.* **42**(4) 638–646.

[23] Williams, T.D., Bennetts, L.G., Squire, V.A., Dumont, D. & Bertino, L. (2013) Wave-ice interactions in the marginal ice zone. Part 1: Theoretical foundations. *Ocean Modelling* **71** 81–91.

[24] Williams, T.D., Bennetts, L.G., Squire, V.A., Dumont, D. & Bertino, L. (2013) Wave-ice interactions in the marginal ice zone. Part 2: Numerical implementation and sensitivity studies along 1D transects of the ocean surface. *Ocean Modelling* **71** 92–101.

[25] Williams, T.D. & Squire, V.A. (2006) Scattering of flexuralgravity waves at the boundaries between three floating sheets with applications. *J. Fluid Mech.* **569** 113–140.